

DESY SR 84-31
November 1984

SURFACE CORE LEVEL SHIFTS OF THE LANTHANIDE METALS

Ce⁵⁸ - Lu⁷¹: A COMPREHENSIVE EXPERIMENTAL STUDY

by

Eigentum der
Property of

DESY

Bibliothek
library

Zugang: 1 1. DEZ. 1984
Accessions:

Leihfrist:

7

7 Tage
days

Loan period:

F. Gerken

IBM Deutschland, Mainz

A.S. Flodström

MAXLAB at Lund University, Lund, Sweden

J. Barth

IBM Research Center, Yorktown Heights, New York

L.I. Johansson

Department of Physics at Linköping University, Linköping, Sweden

C. Kunz

Hamburger Synchrotronstrahlungslabor HASYLAB at DESY, Hamburg

ISSN 0723-7979

NOTKESTRASSE 85 · 2 HAMBURG 52

DESY behält sich alle Rechte für den Fall der Schutzrechtserteilung und für die wirtschaftliche Verwertung der in diesem Bericht enthaltenen Informationen vor.

DESY reserves all rights for commercial use of information included in this report, especially in case of filing application for or grant of patents.

To be sure that your preprints are promptly included in the
HIGH ENERGY PHYSICS INDEX ,
send them to the following address (if possible by air mail) :

DESY
Bibliothek
Notkestrasse 85
2 Hamburg 52
Germany

SURFACE CORE LEVEL SHIFTS OF THE LANTHANIDE METALSCe⁵⁸ - Lu⁷¹: A COMPREHENSIVE EXPERIMENTAL STUDY

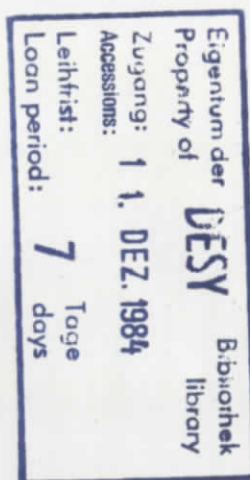
F. Gerken a), A.S. Flodström b), J. Barth c), L.I. Johansson d) and C. Kunz e).

- a) IBM Deutschland, Hechtsheimer Str. 2, 6500 Mainz 1, FRG.
- b) MAXLAB at Lund University, P.O. Box 725, 220 07 Lund, Sweden.
- c) IBM Research Center, P.O. Box 218, Yorktown Heights, New York 10598, USA.
- d) Department of Physics at Linköping University, 581 83 Linköping, Sweden.
- e) HASYLAB at DESY, Notkestrasse 85, 2000 Hamburg 52, FRG.

ABSTRACT

Synchrotron radiation excited photoelectron spectra of the 4f emission region for all lanthanide metals Ce⁵⁸ to Lu⁷¹ (except Pm⁶¹) have been recorded. Photon energies ranging from 30 eV to 200 eV have been used to excite the 4f electrons with maximum surface sensitivity. The 4f emission spectra of all metals studied, with the exception of Ce, show 4f emission from the surface layer atoms and the bulk atoms as clearly separated structures with different binding energies. For Ce no unambiguous separation of the 4f structure into bulk and surface emission could be made. We fitted the experimental spectra with calculated 4f emission spectra obtained by adding a bulk and a shifted surface multiplet for each metal. The intensity ratios within the multiplets were obtained from an atomic calculation utilizing the intermediate coupling scheme. The intensity ratio between bulk and surface emission (I_B/I_S) and the magnitude of the surface core level shift (SCS) were used as fit parameters.

The deduced SCSs are all positive (towards higher binding energy), 0.40 eV - 0.77 eV, and in fair agreement with calculated SCSs using the Johansson - Mårtensson - Rosengren model. For the trivalent lanthanides we found a systematic variation of the SCSs through the series, which can be attributed to differences in the actual electron distribution between s, p and d- like valence states. For the trivalent Sm we found the surface to be completely divalent and deduced a surface shift of > 0,46 eV, being the energy necessary to change the surface valency.



I INTRODUCTION

When high resolution photoelectron spectrometers come into use, it was shown that the binding energies for core levels in atoms strongly depended on their chemical surrounding "chemical shift", (1,2). One of the most fundamental of these chemical shifts is observed between the atoms and the solid, but even more subtle changes in the chemical surrounding of an atom as e.g. a change in coordination number for one atom in different molecules is clearly recognized as a chemical shift in the core level binding energy. These chemical shifts have formed the basis for extremely fruitful research within many fields of science, and much theoretical work has been devoted to relate the observed chemical shifts to physical parameters as e.g. oxidation number, electronegativity etc.

For an elemental solid it was recognized that the surface atoms have another coordination number than the bulk atoms and must experience a different potential. Core levels of the surface atoms should therefore also be expected to exhibit a chemical shift compared to the bulk atoms. This is perhaps easiest understood for solids where directed bonding is strong e.g. covalent semiconductors and transition metals, but also calculations for free-electron like metals show that the potential near the surface is substantially different from the bulk (3).

The idea of a surface atom core level shift (SCS) is old, but was proved only recently to be experimentally observable. Citrin et al. (4) used high resolution XPS (x-ray photoelectron spectroscopy), where the surface sensitivity was enhanced by detecting emitted electrons at grazing angles of emission with respect to the surface. By this method they measured the SCSs of the Au (4f), Ag (3d) and Cu (2p) core levels. Tran Min Duc et al. (5) exploited synchrotron radiation to excite the 4f core level in W, and by variation of the excitation energy the kinetic energies of the excited electrons could be kept in a range where the inelastic electron scattering length is close to its minimum (6). In their data the contrast between surface and bulk emission is therefore very high. This work stimulated synchrotron radiation researchers to a number of investigations of SCSs, primarily of the 4f levels in the 5d transition metals (5, 7-9).

Using synchrotron radiation they could tune the kinetic energies of the electrons to achieve a high surface to bulk contrast.

The interest to measure surface core level shifts was also stimulated by the theoretical work by Johansson, Mårtensson and Rosengren (10, 11) who introduced a thermodynamical model based on a Born-Haber cycle to calculate SCSs for metals. The JMR model only needs the surface energies of the element measured (Z) and the consecutive element (Z+1) in the periodic system to calculate the shift. This has renewed the interest in surface energies and especially theoretical, experimental and empirical ways of estimating them.

We have earlier reported results on the SCSs of the lanthanide 4f levels (12). Our interest was triggered by the very different 4f multiplet structures observed in the 100 eV photon energy synchrotron radiation spectra as compared to the XPS-spectra (13). The present paper reports on a comprehensive study of the SCSs for all lanthanide metals from Ce⁵⁸ to Lu⁷¹ with the exception of Pm⁶¹.

The lanthanides have 4f levels which are localized and core-like even though their binding energies are shallow and sometimes even degenerate with the valence bands. The 4f structures in the photoemission spectra are also relatively sharp and surface core level shifts should be detectable. This was realized early by experimental studies of the Yb 4f level (14).

On the other hand, there are also specific problems related with the 4f-emission of the lanthanides. It is in the lanthanide series where the 4f level is being filled, and hence for most lanthanides the 4f level is only fractionally occupied. An excitation of a 4f electron from 4fⁿ ground state then leaves the atom in a number of different 4fⁿ⁻¹ final states, all of which occur with certain probabilities (15, 16). The complexity of the final state multiplet structure will vary with the 4f occupation number, and only Ce (4f⁰), Yb and Lu (4f¹⁴) represent simple cases.

For all other lanthanides the detailed knowledge of the 4f multiplet structure is essential to analyze photoemission spectra in terms of surface and bulk emission.

Recently, Gerken calculated the energy separation and fractional percentage intensities of the final state 4f multiplet lines for all the lanthanide metals within the intermediate coupling scheme (17). This scheme gives a proper description of the multiplets for all the lanthanides, and the results are essential to fit the experimentally recorded spectra in order to deduce the SCS's.

Experimentally we have only studied evaporated films. These films are polycrystalline to their nature and we should expect different SCSs for different crystal grains (11). The polycrystalline films thus complicate the interpretation of the results and obtaining data from clean lanthanide single crystals has high future priority. We should stress that in our efforts to obtain the SCSs of the lanthanides we have very much benefitted from the earlier XPS work of Lang et al. (13). They obtained excellent XPS-spectra for the lanthanides showing the bulk multiplet structures. In all cases we have used their bulk parameters as starting parameters in the fits of our surface sensitive spectra.

The SCSs obtained for the trivalent lanthanides increase in magnitude going from Ce⁵⁸ to Lu⁷¹ while the JMR model using available thermodynamic data predicts one common SCS for the trivalent lanthanides (18). The JMR model gave SCSs for the 4f levels of the 5d transition metals that agreed well with experiments (7 - 9). The 5d series is characterized by a filling of the 5d valence level and changes in bonding (surface energies) due to this filling. For the trivalent lanthanides in the 4f series the number of valence electrons stay constant when filling the 4f core level. Our results indicate that even if the number of valence electrons are the same, the different distributions of these electrons among s,p and d like valence levels substantially influence the SCSs.

II EXPERIMENTAL

The experiments were performed at the Flipper station, HASYLAB. The monochromator (Flipper) is a plane grating monochromator with a high photon flux at very good energy resolution (19, 20). The emitted electrons were energy analyzed in a double pass cylindrical mirror analyzer. We set the monochromator slits and the analyzer pass energy to get a total energy resolution of < 0.3 eV below 200 eV photon energy. Spectra recorded at 100 eV could be obtained with a total energy resolution of typically 0.15 eV.

The samples were evaporated in situ, the base pressure in the UHV sample chamber being 1×10^{-10} Torr (7.5×10^{-9} Pa). During the evaporations the pressure rose and stabilized at $5 - 8 \times 10^{-9}$ Torr ($4 - 6 \times 10^{-8}$ Pa), after completed evaporation it quickly went back to the starting value. The cleanliness of the samples was at an early stage checked by Auger electron spectroscopy, the contaminants were found to be mainly C1 and O. During the measurements the sample cleanliness was checked by 40 eV photoemission valence band spectra, where the intensity of a structure at 5 - 7 eV binding energy was recognized as contamination derived for most lanthanides. In spite of substantial efforts to obtain absolutely clean films we could for all lanthanides always detect a small contamination derived structure at about 6 eV binding energy and we assume that this is an inherent property of the used evaporation material (21).

The structures in the recorded spectra were fitted using DS lineshape peaks and we used a Gaussian broadening function for the experimental resolution. Except for the experimental broadening, there was no need to introduce an extra Gaussian phonon broadening. This is consistent with the theoretical work by Flynn (22). The shape of the background was calculated from a simple model for inelastic electron scattering (23). The operations necessary to obtain a fit spectra were performed using a computer program developed at HASYLAB. The quality of the fits were judged by visually comparing the experimental spectrum and the corresponding calculated fit spectrum.

We stress that there is an intimate connection between the background intensity and the asymmetry i.e. if we fit the 4f structures not adding any background intensity the asymmetries obtained will differ very much from XPS values. Thus we vary the intensity of the background and the asymmetry simultaneously to get the best fits of the experimental spectra, while constraining the asymmetries to be close to the corresponding XPS ones.

III THEORY

Johansson, Mårtensson and Rosengren (10, 11, 18) have presented a theoretical model, which includes both the initial and the final state effects to predict SCS's. The model is based on a thermodynamical Born-Haber cycle of the photoionization process. They use the equivalent core approximation of the fully screened core hole and obtain to first order.

$E(Z)$ and $E(Z+1)$ are the surface energies of the element investigated and the consecutive element in the periodic table. The surface energy is defined as the difference between the bulk and the surface cohesive energies. The problem of calculating a certain $\Delta E_c(s-b)$ (SCS) is reduced to obtain reliable surface energies of the elements. Only a few a priori calculations of surface energies exist (3, 24) and the experimental surface energies reported from different experiments are very scattered for the same elements and are also usually measured at the melting points (25, 26). For the lanthanides neither experimental nor calculated surface energies of reasonable quality have been published.

Using a semiempirical relation based on the difference in coordination numbers between a surface and a bulk atom, the surface energy has been expressed as a constant fraction of the bulk cohesive energy (27, 28) and eq. (2) can be rewritten as.

Eq. (3) has been used to estimate SCSs for the 4f core levels of the 5d transition metals (11) and we will here apply it to the lanthanides. The use of eq. (3) to calculate the SCS's for the lanthanides poses some problems. The lanthanide series is characterized by a gradually filling of the 4f level, these 4f electrons are localized and at a finite binding energy, thus the 4f orbitals do not represent the screening orbitals of the photoionization process. The screening orbitals are delocalized and at the Fermi level. Consequently the divalent lanthanides have a metallic initial state as $(spd)^2$ and a screened trivalent final state as $(spd)^3$, the trivalent lanthanides have corresponding trivalent $(spd)^3$ initial and tetravalent $(spd)^4$ final states. To apply eq. (3) we need the metallic cohesive energies for the divalent, trivalent and tetravalent states of the lanthanides.

For most of the lanthanides the 4f occupation differs between the atomic and metallic states i.e. a $4f^{n+1} s^2$ to a $4f^n (spd)^3$ transition takes place in the condensation. Exceptions are Eu and Yb which stay divalent, and also Ce, Gd and Lu which are trivalent both in the atomic and the metallic states. Since the bulk cohesive energies reported in tables refer to the atomic ground state and the cohesive energies in eq (3) are to be associated with the valence band cohesive energies in the metallic state we have to estimate the energy associated with the $4f^{n+1}$ to $4f^n$ transition.

This can be accomplished in at least two ways: First we can use the cohesive energies of those lanthanides not changing their 4f occupation number between the atomic and metallic states as fix points and interpolate between them. For the divalent state we have Eu and Yb, for the trivalent state we have Ce, Gd, and Lu. There exist no lanthanide in the tetravalent state but Hf, the next element to Lu, is a good choice for the tetravalent valence state. In Fig. 1 we display the result of the interpolation from which we derive for the divalent, trivalent and tetravalent metallic states the cohesive energies of 40 kcal/mol, 100 kcal/mol and 145 kcal/mol, respectively.

We could also use optical atomic spectra to obtain the excitation energies for the $4f^{n+1}$ to $4f^n$ transition and add these energies to the cohesive energies of the lanthanides with respect to the atomic state (29). This procedure will yield essentially the same result as the interpolation scheme devised, but is somewhat arbitrary because we have to choose a certain valence configuration for the final state. A valence configuration which then should be based on a bandstructure calculation.

If we insert the interpolated metallic cohesive energies in eq. (3), we obtain $a\Delta E_c(s-b)$ (SCS) = 0.50 eV for the divalent lanthanides (Eu and Yb) and $a\Delta E_c(s-b)$ (SCS) = 0.40 eV for the trivalent lanthanides (Ce, Pr, Nd, Gd, Tb, Dy, Ho, Er, Tm and Lu).

In the above treatment we have neglected the possibility that our fix point lanthanide metals may have the same number of valence electrons but not exactly the same valence configuration, i.e. the distribution between s, p and d orbitals may vary through the series. We know from several physical parameters as crystal structure, melting points, hcp-bcc phase transition temperatures, and response to pressure, that the valence configurations are not exactly identical for all the trivalent lanthanide metals. We illustrate the possible consequences of this in Fig. 2, where we assume La to have $s^2 d^2$ and Lu to have $s^{1.6} d^{1.4}$ valence configurations. Observe that although La and Lu are both trivalent in the atomic and metallic states and have almost identical bulk cohesive energies with respect to their atomic states they still have different valence band cohesive energies.

In this paragraph we have illustrated some of the difficulties to obtain reliable estimates of the surface energies for the lanthanides. We have introduced a scheme to estimate metallic bulk cohesive energies which can be used to calculate SCS's for the lanthanides from eq. (3), but there remain some ambiguities associated with this method.

IV EXPERIMENTAL RESULTS

a) The divalent lanthanides; Eu and Yb

The rare earth metals with two valence electrons are Eu ($4f^7$) and Yb ($4f^{14}$), the valence configurations being $(5d\ 6s)^2$. In Yb the 4f shell is completely filled and in the photoemission spectrum of the 4f level we expect two peaks corresponding to the final states of the 4f configuration ($^2F_{7/2}$, $^2F_{5/2}$) with a statistical intensity ratio 4/3. In Fig. 3a we show an XPS-spectrum from Lang et al. (13). In this we see the expected 4f peaks at 1.3 eV ($^2F_{7/2}$) and 2.6 eV ($^2F_{5/2}$) binding energies, respectively. The solid curve drawn through the experimental data points in the XPS-spectrum is a convolution of DS lineshape peaks with a Gaussian broadening function representing the reported experimental resolution of 0.25 eV. We will later discuss the values of the linewidth (γ) and asymmetry (α) parameters of the DS peaks, both the ones reported in ref. (13) and the ones used in this work.

The top curve in Fig. 3a represents the photoemission spectrum recorded at 100 eV photon energy. We clearly see an extra doublet positioned at 0.6 eV higher binding energy compared to the original 4f doublet. The new doublet displays the same intensity ratio (4/3) but is considerably broader than the original one. The main difference between the XPS-spectrum (AlK α , 1486.6 eV) and the 100 eV spectrum is the kinetic energy of the excited electrons. The inelastic electron scattering length at kinetic energies of 1500 eV is considerably larger than for electrons having only 100 eV kinetic energies. The 100 eV spectrum is thus much more surface sensitive than the XPS-spectrum. Therefore we interpret the extra doublet as due to the 4f final states of the surface atoms ($^2F_{7/2}$ (surface), $^2F_{5/2}$ (surface)).

The surface character of the extra doublet is clearly seen in Fig. 4 where we show a number of spectra recorded at different photon energies. We observe a rather drastic increase in the intensity of the surface doublet relative to the bulk doublet as we decrease the photon energy. This is associated with the smaller scattering lengths for lower kinetic energy electrons. In fact one should expect that when we arrive at very low kinetic energies of the electrons (< 15 eV), that the inelastic electron scattering length should start to increase again. We have not been able to observe this expected decrease in the surface sensitivity for the lowest photon energies used in the present investigation of the lanthanides (30). This is in contrast to other data reported (31).

In Fig. 4a we also show the fits obtained using the procedure described earlier. The fits were made using a binding energy difference of 0.6 eV between the surface and the bulk doublet and adjusting the I_B/I_S ratio for different photon energies while keeping the intensity ratio 4/3 fixed within each doublet. At low photon energies we observe a discrepancy in the relative intensities within the doublets. This is a cross-section effect, the 4f cross-section rises from threshold roughly proportional to $hw - E_B^F$. Since E_B^F varies within the 4f multiplets we can observe intensity differences in our experimental spectra not reproduced by our fitting procedure. We should also be aware of that the branching ratio can vary rather more dramatically close to threshold where the final state wave functions are not at all free-electron like (32).

The fit procedure contains two adjustable parameters which can be deduced from our experiments: The magnitude of the SCS and I_B/I_S . If necessary we also changed lineshape parameters for which XPS-values served as starting values, these changes were associated with changes in the intensity of the added background.

In Fig. 3b we show two photoemission spectra of the 4f level in Eu, one XPS-spectrum (13) and the other recorded at 100 eV photon energy. Eu has the $4f^7$ configuration, the final states for the excited $4f^6$ configuration are 7F_J ($J=0,1,\dots,6$) i.e. 7 possible states. In Fig. 3b the calculated intensities and the energy separations for these levels are shown. The solid curve in XPS-spectrum is the result of adding these seven $4f^6$ lines each of which has been convoluted with a DS peak and the sum has been resolution broadened. In the XPS-spectrum and the 100 eV spectrum we observe a maximum 4f intensity at 2 eV binding energy, but in addition we observe in the 100 eV spectrum on the high binding energy side a shoulder which again originates from the 4f electrons of the surface atoms. To represent the experimental 100 eV spectrum we then have to use two sets of 7F_J states i.e. 14 states with the multiplet line intensities given within each set. Finally we show in Fig. 4b fits of this type for a number of photon energies, all parameters frozen except for the I_B/I_S ratio which was varied to simulate the different surface sensitivities for different photon energies. Also our photon energy resolution varies between the spectra, an effect which is included as a variable Gaussian contribution to the lineshape in the fitting procedure. We show the single fit components for the 30 eV spectrum; bulk peak, surface peak and background contribution. Here we obtain a SCS of 0.63 eV (Yb:0.60 eV) and also we observe a surface peak being much broader than the bulk peak.

b) The light trivalent lanthanides; Ce, Pr and Nd.

In Figs 5a - c we show XPS-spectra for Ce, Pr and Nd (13) compared to our 100 eV spectra. Unlike for Eu and Yb, no clearly separated surface structures are observed. The surface core level shifts predicted by the JMR model are 0.4 eV for all trivalent lanthanides. For Ce, Pr, and Nd the lifetime broadening as determined from the XPS-spectra are of the same order of magnitude, 0.4 - 0.5 eV (Table I). Therefore any SCS will be hard to observe, and we must rely on fits to separate the 4f structures into bulk and surface peaks.

For Ce, Parks et al. (33) have obtained a good fit of their experimental spectra using a bulk and a surface peak separated by 0.3 eV. They give an upper limit for the SCS of Ce to 0.4 eV. They also succeeded to obtain a constant binding energy of 1.85 eV for the bulk peak when fitting spectra recorded at different photon energies. To prove the existence of a SCS for Ce, we have to compare such a fit with a single peak fit. In Fig. 6 we show spectra for three different photon energies and the fits obtained by adding just one Lorentzian peak and a background. We have fitted the structure at 2 eV binding energy which has been shown to clearly exhibit 4f-character (23, 34 - 36). The quality of the fit is limited due to overlapping valence band emission. Reasonable agreement is found for a Lorentzian of 0.45 eV HWHM. The binding energy also stays constant for different photon energy spectra and we obtain a binding energy of 2.01 ± 0.02 eV for all spectra. We conclude that we have no possibility to unambiguously give a definite value for the SCS in the case of Ce, especially since the XPS-spectrum gives no clear information on the binding energy and the lineshape of the 4f peak (13).

For Pr which shows a structureless 4f peak at all our photon energies we have tried to fit the 40 eV and 100 eV spectra with only a bulk peak, but also by adding a bulk and a surface peak. The results are shown in Fig 7a and b, the fits are of comparable quality. But there are clear indications that only using a bulk peak is not correct. In this case the bulk peak is fitted with a Lorentzian having HWHM of 0.55 eV which is significantly broader than the corresponding HWHM of the 4f peak in the XPS-spectrum. This is in contrast to our findings for the other lanthanides where our bulk parameters generally show a very good agreement with the XPS-spectra parameters. Furthermore we have to shift the bulk peak from a binding energy of 3.50 ± 0.02 eV in the 40 eV spectrum to 3.45 ± 0.02 eV in the 100 eV spectrum to obtain a good fit using a single bulk peak, while using a bulk and surface peak we obtain a constant binding energy for the bulk $2F_{5/2}$ multiplet peak for all photon energies.

For Nd the situation is clearer because even the raw data display a change in the 4f-structure for different photon energies (Fig. 8). Fitting the spectra by adding bulk and surface peaks yields bulk parameters close to the XPS-values. However, for Nd and especially for Pr the deduced magnitude of the SCS depends stronger on our choice of lineshape parameters than for Yb and Eu. Therefore we quote an error of ± 0.1 eV for the SCS of Nd and Pr. The fitting parameters are summarized in Table I.

For Ce the analogy to the other lanthanides certainly suggests the existence of a SCS. For reasons outlined above our experimental data do not allow us to ascribe it any specific value between 0 and 0.4 eV.

c) The heavy trivalent lanthanides; Gd, Tb, Dy, Ho, Er, Tm and Lu.

In Figs 9 a-g we compare XPS-spectra with 100 eV photon energy spectra. We first discuss Gd ($4f^7$) and Lu ($4f^{14}$) which have the same 4f-configurations as the divalent Eu ($4f^7$) and Yb ($4f^{14}$). We thus expect 4f spectra of similar appearance for Gd, Eu and Lu, Yb, respectively. In fact, the main differences in the XPS-spectra are the absolute 4f binding energies, which are higher for Lu and Gd due to the higher atomic numbers compared to Yb and Eu, and the larger lifetime widths for Lu and Gd which is related to their higher binding energies. The larger lifetime widths make the visibility of the surface shifted 4f peaks somewhat worse, but still they are seen as an extra doublet in the 100 eV spectrum of Lu and as an asymmetry on the high binding energy side of the Gd 4f peak in its 100 eV spectrum (Figs 9 a and b).

The elements Tb ($4f^8$) through Tm ($4f^{12}$) show strong multiplet splittings in their 4f photoemission spectra (Figs 9 c - g). For Tb and Dy the multiplet lines divide into two sets, the one with lower binding energy represents final states with maximum total spin for the 4f configuration and displays only few components. Here it is easy to conclude that also Tb and Dy have surface 4f emission.

For Ho, Er and Tm differences between XPS and 100 eV spectra only show up as different relative intensities between different parts of the multiplets. Any additional peaks that can be assigned to surface emission only are hardly detected. We have observed earlier that the bulk parameters obtained from XPS-spectra very well represent the bulk emission excited with 100 eV photon energy (see Eu and Yb). It is therefore fairly safe to assume that the change in relative intensities from the XPS-spectra to the 100 eV spectra is due to shifted surface multiplets in the 100 eV spectra overlapping the bulk multiplets. To obtain an estimate of the SCSs we have to rely on our fitting procedure i.e. we use calculated multiplet splittings and relative intensities and add a surface and a bulk multiplet with different energy separations to obtain the best representation of the experimental spectrum considered. The results of such fitting procedure are plotted for Gd to Lu in Figs. 10 a - g. To minimize possible ambiguities we fitted a number of spectra at different photon energies with fixed line-shape parameters for each metal allowing only the I_B/I_S ratio, the background intensity, and the resolution broadening to vary. The SCS's obtained for Gd to Lu together with the used fit parameters are summarized in Table I. As already observed for the divalent Eu and Yb, the surface related peaks show additional broadening. In some of the fits there is a discrepancy between the relative intensities measured and calculated for different multiplet lines. We attribute this to the variation of the 4f crosssection as a function of the photoelectron's kinetic energy, i.e. multiplet lines with different binding energies have different crosssections for the same excitation energy.

d) Valence change at the Sm surface

For Sm, surface sensitive photoemission experiments have shown that the surface atoms have a different 4f configuration than the bulk atoms (37 - 39). In the bulk Sm is trivalent ($4f(5d6s)^3$) and at the surface Sm is divalent ($4f(5d6s)^2$).

Lang and Baer concluded from combined XPS and Bremsstrahlung-Isochromat-Spectroscopie (BIS) measurements that the valence change was driven by a downward surface shift of the unoccupied $4f^6$ multiplet to a position below E_F (39). In Fig 11 we show the XPS spectrum of Sm together with spectra obtained at 35 eV and at 100 eV photon energy. The energy position of the empty $4f^6(^7F_0)$ multiplet is also indicated. The sum of the binding energy of the first multiplet line of the final state $4f^5$ configuration of at the Sm surface occupied $4f^6$ configuration (0.77 eV) and the energy position above E_F of the first multiplet line of the Sm bulk unoccupied $4f^6$ final state configuration of the BIS measurements (0.46 eV) can be taken as the SCS of the Sm surface atoms. However, we should observe that only 0.46 eV is needed to cause a valence change, the additional binding energy of 0.77 eV for the occupied $4f^6$ multiplet most likely originates from the valence change itself (40).

The large energy separations between the unoccupied $4f^6$ multiplets and E_F was taken as experimental evidence that the Sm surface must be completely divalent and the bulk completely trivalent (39). This is in contrast to earlier interpretations of the Sm surface to be of mixed valence (37, 38). The present study strongly supports the view of a single valency for the Sm surface. Any amount of trivalent Sm surface atoms should show up as a surface shifted $4f^4$ multiplet final state configuration. Our spectra show clearly a trivalent bulk multiplet structure ($4f^5$ to $4f^4$) and a divalent surface multiplet structure ($4f^6$ to $4f^5$), the sum of these two multiplets with calculated intensity differences within the multiplets and properly broadened gives very good account of the experimental data. There is no sign of a surface trivalent multiplet separated by at least 0.46 eV from the bulk multiplet (Fig. 12).

The intensity ratio between bulk and surface emission, I_B/I_S , obtained from the 100 eV spectrum is 1.23 which is in reasonable agreement with the assumption of a completely divalent surface. We had to use somewhat different DS line shape parameters to fit the 4f to 4f multiplet than reported earlier (13). Several effects may be responsible for this observation. Different theoretical multiplet intensities were utilized in the fits.

In contrast to Ref 13, we calculated the multiplet intensities in the intermediate coupling scheme (17). A physical effect due to our surface sensitivity could also add to the discrepancy i.e. a small SCS for the second layer atoms may exist not large enough to cause a valence change but sufficient to contribute to a broadening and increased asymmetry of the bulk multiplet in the 100 eV spectrum. Yet, the completely divalent character of the Sm surface is clearly established.

V DISCUSSION

The SCSs for all the lanthanides studied and the parameters for the bulk and surface core level peaks given by the fits are shown in Table I. Also given are the energy scaling factors i.e. the numbers used to multiply the atomically calculated energy separations between the different multiplet lines to obtain correspondence with the differences measured for the solid lanthanides. In the case of Sm the energy scaling factors are different for the bulk and the surface emission, as the surface has another 4f occupation. For Eu and Gd with a very small multiplet splitting (0.06 eV) is the determination of an energy scaling factor difficult. Our parameters obtained for the bulk emission are for Eu and Gd identical with the bulk parameters obtained from XPS-spectra, we have consequently chosen the same multiplet splittings as reported for the XPS-spectra (13). For Gd using this splitting made it possible to fit the broad asymmetric 4f peak by only varying the surface emission parameters. In Fig. 13 we graphically display the bulk and surface parameters given in Table I and compare them with the bulk parameters obtained from the XPS-spectra (13). Especially for the heavier lanthanides, Tb to Tm bulk parameters deduced from XPS-spectra differ somewhat from bulk parameters deduced from the spectra recorded at lower photon energies (100 eV), where a separation of bulk and surface emission had to be made. This is partly due to the relative multiplet intensities used in the fits. We have used relative intensities calculated in the intermediate coupling scheme (17), which for the heavier lanthanides should give a more adequate representation of the experimental data than the relative multiplet intensities calculated using the LS coupling scheme (16).

The main observation in Table I and Fig. 13 is that the surface emission parameters differ substantially from the bulk emission parameters. In the fitting procedure we could often get equivalent quality for fits with very different surface emission parameters, if we simultaneously allowed for a variation in the SCSs. The parameters given in Table I are the ones used in the fit curves displayed in the figures of section IV. These parameters can for the surface emission be varied about 20% and we still get satisfactory fit curves keeping the SCSs within the limits quoted in Table I, larger variations in the surface emission parameters will not produce good fits.

For the lifetime broadening, γ (HWHM), we observe in general a larger value for the surface emission than the corresponding bulk emission, this fact is not influenced by our quoted error limits. From Fig. 13 we can see that for the surface emission the HWHM varies strongly along the 4f series but one cannot deduce any trend. Similar surface emission broadening has been observed for polycrystalline Na and Mg (41), but for polycrystalline Au, Ag and Cu identical bulk and surface lineshape parameters could be used to obtain good fits of surface sensitive XPS-spectra (4). From surface sensitive measurements of the Au 4f peak using synchrotron radiation, it was shown that the broader surface emission peak obtained for polycrystalline Au could be fitted under the assumption, that the different single crystal grains in the evaporated film had different SCSs (42). Identical bulk and surface emission parameters could then be used and the SCSs quoted for different grains were in good agreement with those given from single crystal data (8).

For the lanthanides there exist no surface sensitive photoemission measurements of the 4f levels from single crystals. We can therefore not decide whether the surface emission broadening observed is an intrinsic effect or due to the polycrystalline nature of our samples. For Lu calculations show that the SCSs are quite different for different single crystal faces (11). These calculations are based on a model which assume dominant d-electron bonding between the atoms in solid Lu, a model which probably holds for all trivalent lanthanides. It is thus very likely that the observed surface broadening for the lanthanides could be explained by the different SCSs for the different single crystal grains which exist on a polycrystalline sample surface.

This hypothesis should be tested experimentally. To try to fit the surface emission structures of the present data with more than one DS peak seems not very useful, since we have no a priori knowledge of either the distribution in number of different single crystal grains in the surface or the actual SCSs for these grains.

Second layer SCSs could be another possible way to explain the broad surface peaks observed. However, there are a number of arguments speaking against this explanation. We believe that the "directed" d-electron bonding is responsible for the SCSs for the trivalent lanthanides. The second layer atoms have all their nearest neighbour bonds satisfied and should be very bulk like. Another mechanism for the SCSs is the Friedel oscillations of the electronic charge near the surface, which also can influence the potential of the surface atoms and cause observable SCSs. This mechanism is valid in the free-electron like metals as Na, Mg and Al (41) and could give a contribution to the SCSs of the lanthanides. This mechanism is also essentially limited to the first layer atoms (3). We therefore believe that the decrease of the SCSs between first and second layer atoms must at least be exponential. The second layer SCS will then be so small that it only broadens the bulk emission as observed in Sm, but not influences the first layer surface emission peaks. Further evidence for second layer emission contributing to bulk peak broadening can be seen in the Lu spectrum of Fig. 9g, where the XPS-spectrum derived bulk parameters do not reproduce the high binding energy side of the 100 eV bulk peak accurately. Since the low binding energy side of the bulk peak still is very steep it is not possible to improve the fit quality by simply increasing the lifetime width of the DS peak. We interpret the high binding energy side bulk peak broadening as due to a small second layer surface shift which do not show up in the XPS-spectrum.

Finally we display in Fig. 14 the SCSs for the polycrystalline lanthanides derived from the fit curves in section IV, we also display the appropriate error limits. We observe that for Eu and Yb, the divalent lanthanides, the experimental SCSs are close to the estimated value (0.5 eV) using eq. (3) and the bulk cohesive energies given in Fig. 1. For the trivalent lanthanides we obtain from eq. (3) and Fig. 1 an estimated SCS of 0.4 eV, which should be the same all trivalent lanthanides. The experimental SCSs instead show a systematic variation from 0.4 eV for Pr to 0.77 eV for Lu.

The trend in the SCSs for the trivalent lanthanides cannot be explained using available thermodynamic data for the surface and the bulk cohesive energies of the lanthanides in eqs. (1) and (3). The application of the model to the lanthanides is as explained in section II complicated by a number of factors. First, we cannot use eq. (1), since there is no reliable theoretical or experimental data on the surface energies of the lanthanides. When we use eq. (3) we need the bulk cohesive energies for the tetravalent (Z+1) and trivalent (Z) state of the trivalent lanthanides with respect to their tetravalent and trivalent atomic states (their metallic bond energies). These numbers are not trivial to obtain, most trivalent lanthanides exhibit a divalent atomic state i.e. in creating the solid a transition $f^{n+1} s^2$ to $f^n (sd)^3$ takes place. In principle this excitation energy is available from optical spectra of the atoms (29), if we assume a given $(sd)^3$ configuration as e.g. $s^2 d$. The largely unknown $(sd)^3$ configuration in the solid lanthanides make this procedure questionable. Another way of estimating the trivalent cohesive energies was devised in Fig. 1. We use the fact that La, Ce, Gd and Lu have trivalent atomic states and interpolate the trivalent metallic cohesive energies for the remaining lanthanides from them. For the metallic cohesive energy of the screened tetravalent state the cohesive energy of Hf is the natural choice not changing its valency going from the atomic to the metallic state and being the Z+1 element to Lu. In Fig. 1 we estimate the tetravalent cohesive energies of the lanthanides by interpolating using the Zr, Hf and Th cohesive energies as fix points. The interpolation yields the same trivalent and tetravalent metallic cohesive energies for all lanthanide metals and will not give any trend in the SCSs along the series.

However, there exist bulk properties connected to the metallic bonding which show a variation along the lanthanide series. In Fig. 15 we plot the melting temperatures, which display a monotonic increase from Ce to Lu. We also observe that the minor energy separating the trivalent and divalent states for bulk Sm and Tm are possible shown as kinks in the melting temperature curve. The energy associated with melting is a small fraction of the cohesive energy and in the melting process we also essentially conserve the metallic electronic configuration. Thus the melting curve behaviour indicates that there must be differences in bonding between the atoms depending upon the actual lanthanide metal we consider. These bonding differences are naturally related to the electronic configuration of the valence band i.e. the distribution of the valence electrons between s, p and d like states may differ. We assume that the 4f electrons are essentially non bonding.

The main difference in the electronic structure of the trivalent lanthanide elements is the number of 5d electrons in the valence band. An energy band calculation correlating crystal structure with d-band occupation yields for La, $n_d = 2.5$ and for Lu, $n_d = 1.5$ (43). A more recent calculation including the hybridisation between s and d-states gives $n_d = 2.0, 1.4$ and 2.3 for La, Lu and Hf, respectively (44). Assuming that the d-electrons are mostly responsible for the bonding and thus for the surface and the bulk cohesive energies we conclude that the SCS of La should in magnitude be between the SCSs of Lu and Hf. Experimentally we observe 0.77 eV for Lu and 0.44 for Hf (45). No SCS measured for La has been reported. If the number of d-electrons decreases monotonically through the lanthanide series, this will give a reasonable explanation for the variation of the SCSs. The explanation is similar to the one used to explain the systematic variation in the SCSs in the 4f levels of the 5d transition metals upon filling the 5d valence band (10). But for the lanthanides we start with a higher d-band occupancy in the beginning of the series, which decreases upon filling the 4f level and we consequently observe an increasing SCS. The main objection is that such variation in the d-band occupation should be reflected the bulk cohesive energies of La and Lu.

Using eq. (3) and Fig. 14, the variation in the bulk cohesive energy should be of the order 15 kcal/mol between the lightest and heaviest trivalent lanthanide. From Fig. 1 there is no support for this, we have however to remember that even for La, Ce, Gd and Lu which are trivalent both as free atoms and as metals there is a valence configuration change going from the atomic to the metallic state (Fig. 2). In other words the reported bulk cohesive energies could have less relevance for the metallic bond energies than expected. It has been convincingly shown that the variation in the d-band occupancy reported yield metallic bond energies which explain the different crystal structures in the lanthanide series (48). Harder to explain without detailed considerations is the variation in properties, which one naively associates with increasing d-electron bonding as hardness and melting temperature, their variation along the series seem to be opposite to the expected behaviour from the picture given.

For the divalent metals, Eu and Yb, the d-occupancy is probably too low for the assumption about the d-electron contribution to the bulk and the surface cohesive energies to be dominant.

In explaining the origin of the SCS variation of the lanthanide metals we have to consider the possibility that it could be of extrinsic origin i.e. the SCSs could be influenced by contamination and different elements could have different susceptibility to e.g. oxygen, which could introduce a variation in the SCS not characteristic of the clean metals. To study this we have recorded spectra of contaminated lanthanide films. For "all" of them we observe stable SCSs and the contamination only decreases the intensity of the surface emission. We noticed one exception to this behaviour, namely Lu. For Lu the SCS observed increased upon oxidation (Fig. 16) and we have to admit that our reported value of 0.77 eV for the SCS in Lu could be lower for a cleaner Lu surface. Extrapolating from our oxidation data we find that the SCS of clean Lu could be as low as 0.70 eV (45). That Lu differs from the other lanthanide elements could be explained by that Lu alone could have a chemisorbed phase of oxygen preceding the bulk oxidation and this chemisorbed phase could alter the Lu surface energy as to shift the surface peak to higher binding energy.

This type of behaviour has earlier been detected for the Al (111) surface (46). We emphasize, that from our data on contaminated films of other lanthanide metals there is no evidence for the variation of the SCS through the lanthanide series to be of extrinsic origin.

VI SUMMARY

We have shown that the 4f levels of all lanthanide metals Ce^{5f} to Lu^{7f} (except Pm^{6f}) exhibit positive SCS i.e. the surface core level peaks are displaced to higher binding energies compared to the corresponding bulk peaks. For the divalent lanthanides, Eu and Yb, of the SCSs are accurately predicted by the JMR model (19) using available metallic cohesive energies. The SCSs of the trivalent lanthanides show increasing SCSs with increasing atomic number. This variation is not predicted by the JMR model which yields the same SCS for all trivalent lanthanides with the metallic cohesive energies deduced. A SCS that at best represents an average of the experimentally measured SCSs for the different trivalent lanthanides. The possible explanation to this trend in the SCSs could be a systematic variation in the d-band occupancy in the valence bands of the trivalent lanthanides.

For Ce, our spectra do not allow us to detect a surface shifted 4f-peak. We believe that the SCS of Ce still awaits a firm determination.

Sm was shown to have a completely divalent surface, the deduced SCS for the hypothetical trivalent Sm surface is found to be > 0.46 eV.

From the lineshapes of the surface and the bulk 4f peaks we observe that the surface peaks are broader. A fact that we attribute to the polycrystalline nature of our surfaces. We find no systematic differences between the bulk and the surface peak asymmetries that could be used in any argument about differences in the electron relaxation processes following a core hole creation in the bulk or at the surface of the lanthanide metals.

Finally the SCS of Lu is found to increase continuously upon oxidation, which makes the observed shift in our spectra of 0.77 eV to an upper limit for the clean metal surface shift. The oxidation behaviour of Lu is unique compared to the other lanthanides metals studied.

ACKNOWLEDGEMENT

We want to thank the staff of HASYLAB for their excellent technical support. This work was supported by the Swedish Board for Natural Sciences and the Bundesministerium für Forschung und Technologie.

REFERENCES

1. K. Siegbahn, C. Nordling, A. Fahlman, R. Nordberg, K. Hamrin, J. Hedman, G. Johansson, T. Bergmark, S.E. Karlsson, I. Lindgren and B. Lindberg, ESCA; Atomic, Molecular and Solid State Structure Studied by Means of Electron Spectroscopy. Nova Acta Regiae Soc. Sci. Upsaliensis Ser IV, Vol 20 (1967).
2. K. Wandelt, Surf. Sci. Reports 2, 1 1982.
3. N.D. Lang and W. Kohn, Phys. Rev. B1, 4555 (1970).
4. P.H. Citrin, G.K. Weertheim, and Y. Baer, Phys. Rev. Lett. 41, 1425 (1978).
5. T.M. Duc. C. Guillot, Y. Lasailly, J. Lecante, Y. Jugnet, and J.C. Yedrine, Phys. Rev. Lett. 43, 789 (1979).
6. R.H. Ritchie, F.W. Garber, M.Y. Nakai, and R.D. Birkhoff, Advan. Radiation Biology 3, 1 (1969).
7. J.F. van der Veen, F.J. Himpsel, and D.E. Eastman, Phys. Rev. Lett. 44, 189 (1980); Solid State Commun. 40, 57 (1981).
8. J.F. van der Veen, P. Heimann, F.J. Himpsel, and D.E. Eastman, Solid State Commun. 38, 595 (1981); 37, 555 (1981).
9. D.E. Eastman and F.J. Himsel, J. Vac. Sci., Technol. 20, 609 (1982).
10. B. Johansson and N. Mårtensson, Phys. Rev. B21, 4427 (1980).
11. A. Rosengren and B. Johansson, Phys. Rev. B22, 3706 (1980).
12. R. Kammerer, J. Barth, F. Gerken, A. Flodström, and L.I. Johansson Solid State Commun. 41, 435 (1982); F. Gerken, J. Barth R. Kammerer, L.I. Johansson, and A. Flodström, Surf. Sci. 117, 468 (1982).
13. J.K. Lang, Y. Baer and P.A. Cox, J. Phys. F11, 121 (1981).
14. S.F. Alvarado, M. Campagna, and W. Gudat, J. Electr. Spectrosc. Rel. Phenom 18, 43 (1980).
15. W.T. Carnall, P.R. Fields and K. Rajnak, J. Chem. Phys. 49, 4412 (1968).
16. P.A. Cox. Structure and Bonding 24, 59 (1975).
17. F. Gerken, J. Phys. F13, 703 (1983).
18. B. Johansson and N. Mårtensson, Helvetia Physica Acta 56, 405 (1983).
19. W. Eberhardt, G. Kalkoffen and C. Kunz, Nucl. Instr. and Meth. 152, 81 (1978).
20. J. Barth, F. Gerken and C. Kunz, Nucl. Instr. and Meth. 208, 307, 1983.
21. It is known that H,O,N,Cl easily move interstitially in the lanthanide metal lattices.
22. C.P. Flynn, Phys Rev. Lett. 37, 1445 (1976).
23. F. Gerken, thesis, Hamburg 1983.
24. M.C. Desjonqueres and F. Cyrot-Lackmann, Surface Sci. 50, 257 (1975).

25. H.H. Wawra, *Materialpruf.* 14, 413 (1972).
26. W.R. Tyson and W.A. Miller, *Surf. Sci.* 62, 267 (1977).
27. A.S. Skapski, *J. Chem. Phys.* 16, 389 (1948).
28. A.A. Lucas, *Collective Properties of Physical Systems* edited by B. Lundqvist, S. Lundqvist and V. Runnström-Reio (Academic Press N.Y. 1973)p 169.
29. L. Brewer, *J. Opt. Soc. of Am.* 61, 1101 (1971).
30. We have recorded data down to a photon energy of 20 eV corresponding to 18eV kinetic energy with respect to E for the Yb 4f electrons.
31. Y. Takakura, S. Takahashi, S. Suzuki, S. Kono, T. Yokotsuka, T. Takahashi and T. Sagawa, *ISSP Activity Report of Synchrotron Radiation Laboratory* (1981).
32. R. Nyholm, A. Berndsson, R. Nilsson, J. Hedman and C. Nordling, *Physica Scripta* 16, 383 (1971).
33. R.D. Parks, N. Mårtensson and B. Reihl, *Int. Conf. on Valence Fluctuations*, Zurich (1982).
34. G. Kalkoffen, thesis, Hamburg 1978.
35. L.I. Johansson, J.W. Allen, T. Gustafsson, I. Lindau and S.B. Hagström, *Solid State Commun* 28, 53 (1978).
36. N. Mårtensson, B. Reihl, and R.D. Parks, *Solid State Commun.* 41, 513 (1982).
37. J.W. Allen, L.I. Johansson, I. Lindau, and S.B. Hagström, *Phys. Rev.* B21, 1335 (1980).

38. G.K. Wertheim and G. Crecelius, *Phys. Rev. Lett.* 40, 813 (1978).
39. J.K. Lang and Y. Baer, *Solid State Commun.* 31, 945 (1979).
40. A. Rosengren and B. Johansson, *Phys. Rev.* B27, 3068 (1982).
41. R. Kammerer, J. Barth, F. Gerken, C. Kunz, S.A. Flodström, and L.I. Johansson, *Phys. Rev.* B26, 3491 (1982).
42. J. Barth, thesis, Hamburg 1982.
43. J.C. Duthie and D.G. Pettifor, *Phys. Rev. Lett.* 38, 564 (1977).
44. H. Skriver, private communication.
45. R. Nyholm and J. Schmidt-May, abstract VII Conf on VUV radiation, Jerusalem (1983).
46. S.A. Flodström, C.W.B. Martinsson, R.Z. Bachrach, S.B. Hagström, and R.S. Bauer, *Phys. Rev. Lett.* 40, 907 (1978).

FIGURE CAPTIONS

Figure 1.

Reported experimental cohesive energies for the elements in the lanthanide series and related elements which do not change their 4f level occupancy between the atomic and the metallic states. The interpolation lines are taken to represent the metallic cohesive energies of the di, tri, and tetravalent states of the lanthanide metals.

Figure 2.

Illustration of the influence of the actual distribution of electrons between s and d-states for the different trivalent lanthanides on their metallic cohesive energies.

Figure 3.

Comparison between XPS-spectra (13) and 100 eV photon energy spectra for the 4f emission region of a) Eu and b) Yb. Also shown are the theoretical multiplet intensities and the calculated fits to the XPS-spectra (solid lines).

Figure 4.

a) Yb 4f emission spectra recorded at different photon energies. The experimental curves are fitted with calculated curves using fixed line-shape parameters and a SCS of 0.60 eV, but varying the I_{4f}/I_{5d} ratio between different photon energies. At the bottom of the figure we show the 100 eV bulk and surface multiplets. The $^2F_{7/2}$ to $^2F_{5/2}$ intensity ratio is fixed to 4/3 for both the bulk and the surface multiplet in all the calculated fit spectra.

b) Eu 4f emission spectra recorded at different photon energies. The experimental curves are fitted with calculated curves using fixed line-shape parameters and a SCS of 0.63 eV, but varying the I_{4f}/I_{5d} ratio between the different photon energies. At the bottom of the figure we show the 30 eV bulk and surface multiplets also shown is the calculated background.

Figure 5.

Comparison between XPS-spectra (13) and 100 eV photon energy spectra for the 4f emission region of a) Ce b) Pr and c) Nd. Also shown for Pr and Nd are the theoretical multiplet intensities and the calculated fits to the XPS-spectra (solid lines).

Figure 6.

Comparison between the experimental spectra and the calculated fit spectra for the 4f emission of Ce. One single Lorentzian peak (HWHM = 0.45 eV) represents the calculated fit spectrum, also shown is the calculated background. The only difference between the fit spectra at the different photon energies is the different resolution broadening (Gaussian).

Figure 7.

a) Comparison between the experimental spectra and the calculated fit spectra for the 4f emission of Pr. Fit spectra obtained by a superposition of the bulk and the surface multiplets with the SCS set to 0.50 eV. At the bottom of the figure we show the separate multiplets curves for the 100 eV spectrum, also shown is the calculated background.

b) Comparison between the experimental spectra and the calculated fit spectra for the 4f emission of Pr. One single DS peak (HWHM = 0.55 eV and $\sigma = 0.05$) represents the calculated fit spectrum, also shown is the calculated background.

Figure 8.

Comparison between the experimental spectra and the calculated fit spectra for the 4f emission of Nd. Fit spectra obtained by a superposition of bulk and surface multiplets, with the SCS set to 0.40 eV. At the bottom of the figure we show the separate multiplets for the 60 eV spectrum, also shown is the calculated background.

Figure 9.

Comparison between XPS-spectra (13) and 100 eV photon energy spectra for the 4f emission regions of a) Gd, b) Tb, c) Dy, d) Ho, e) Er, f) Tm and g) Lu. Also shown are the theoretical multiplet intensities and the calculated fits to the XPS-spectra (solid lines).

Figure 10.

Comparison between the experimental spectra and the calculated fit spectra for a) Gd, b) Tb, c) Dy, d) Ho, e) Er, f) Tm and g) Lu. Fit spectra obtained by superposition of bulk and surface multiplets. At the bottom of the figures we show the separate bulk and surface multiplets for the lowest photon energy spectra, also shown are the calculated backgrounds.

Figure 11.

Comparison between an XPS-spectrum (13) and two spectra recorded at 35 eV and 100 eV photon energy of the 4f emission region of Sm. Also shown are the multiplet intensities for the bulk emission ($4f^5$ to $4f^4$), the surface emission ($4f^6$ to $4f^5$) and the bulk BIS transition ($4f^5$ to $4f^6$).

Figure 12.

Fit of the Sm experimental spectrum at 100 eV photon energy by an addition of the bulk and the surface multiplet emissions. The bulk and surface multiplets are shown separately at the bottom of the figure, also shown is the calculated background.

Figure 13.

HWHM (γ) and asymmetries (α) for the DS peaks used in the fits of the 4f emission spectra displayed in section IV. X, bulk parameters (13); 0, bulk parameters (present work); 0, surface parameters (present work).

Figure 14.

SCSs obtained from the fits reported; 0, divalent lanthanides; 0, trivalent lanthanides. The 0.3 eV value for Ce is reported in (33), we are not able to make a certain statement about the actual the SCS between the limits 0 and 0.4 eV. Also shown are the estimated SCSs for the di- and trivalent lanthanides using the bulk cohesive energies from Fig. 1 and relation (3).

Figure 15.

Melting temperatures for the lanthanide metals (solid curve). We also display the estimated surface energies from the melting temperatures (dashed curve).

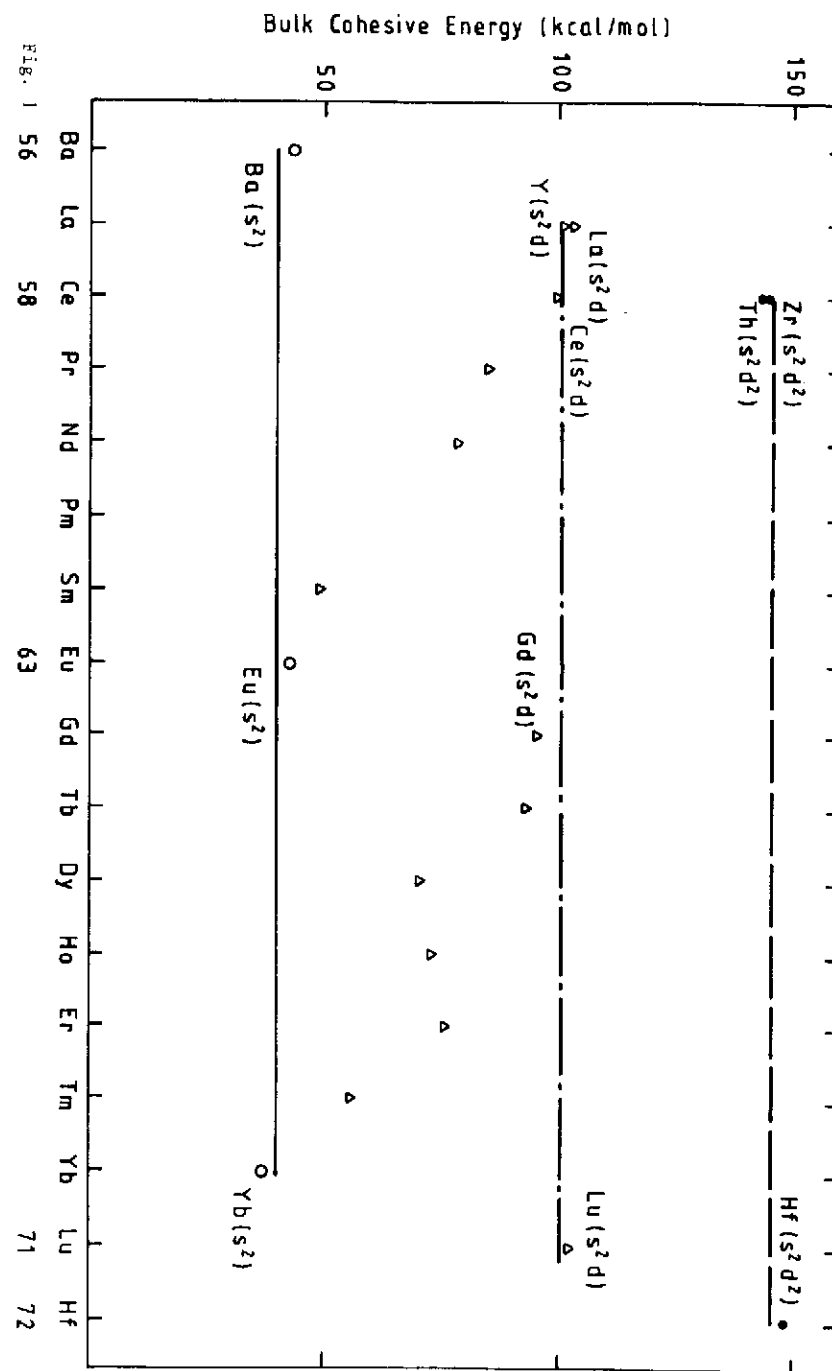
Figure 16.

Two experimental spectra of the 4f emission for Lu obtained at two different stages of contamination, upper curve contaminated and lower curve clean. The contamination derived structure due to O2p or C1 2p is observed at $E_B^F = 6$ eV. Note the increase in the SCS upon increased degree of contamination.

TABLE I

Element	Bulk		Surface		SCS $\Delta E_C(s-b)(eV)$	Energy scaling factor
	HWHM $\gamma(eV)$	Asymmetry α	HWHM $\gamma(eV)$	Asymmetry α		
Ce	0.45	0				
Pr	0.40	0.07	0.40	0.07	0.4 ± 0.1	1.10
Nd	0.38	0.12	0.50	0.10	0.5 ± 0.1	1.10
Sm	0.19	0.13	0.26	0.10		1.11/0.97*
Eu	0.06	0.18	0.13	0.22	0.63 ± 0.03	0.97
Gd	0.15	0.19	0.25	0.07	0.50 ± 0.05	1.25
Tb	0.15	0.15	0.30	0.15	0.55 ± 0.05	1.11
Dy	0.16	0.13	0.25	0.15	0.55 ± 0.05	1.11
Ho	0.13	0.20	0.22	0.22	0.63 ± 0.05	1.075
Er	0.14	0.12	0.30	0.12	0.65 ± 0.05	1.11
Tm	0.08	0.23	0.35	0.25	0.70 ± 0.05	1.11
Yb	0.05	0.13	0.20	0.12	0.60 ± 0.03	1.0
Lu	0.06	0.22	0.45	0.10	0.77 ± 0.07	1.14

Doniach-Sunjic lineshape parameters for the bulk and surface 4f emission of the lanthanides. Also shown are the SCS's with appropriate error limits. The lineshape parameters can be changed 10% and 20% for the bulk and surface emission, respectively, and still yield acceptable fits. The energy scaling factor is needed to multiply the atomic theoretical multiplet splittings to get good fits of our solid state spectra. The * for Sm recognizes the surface emission which have another 4f configuration than the bulk emission.



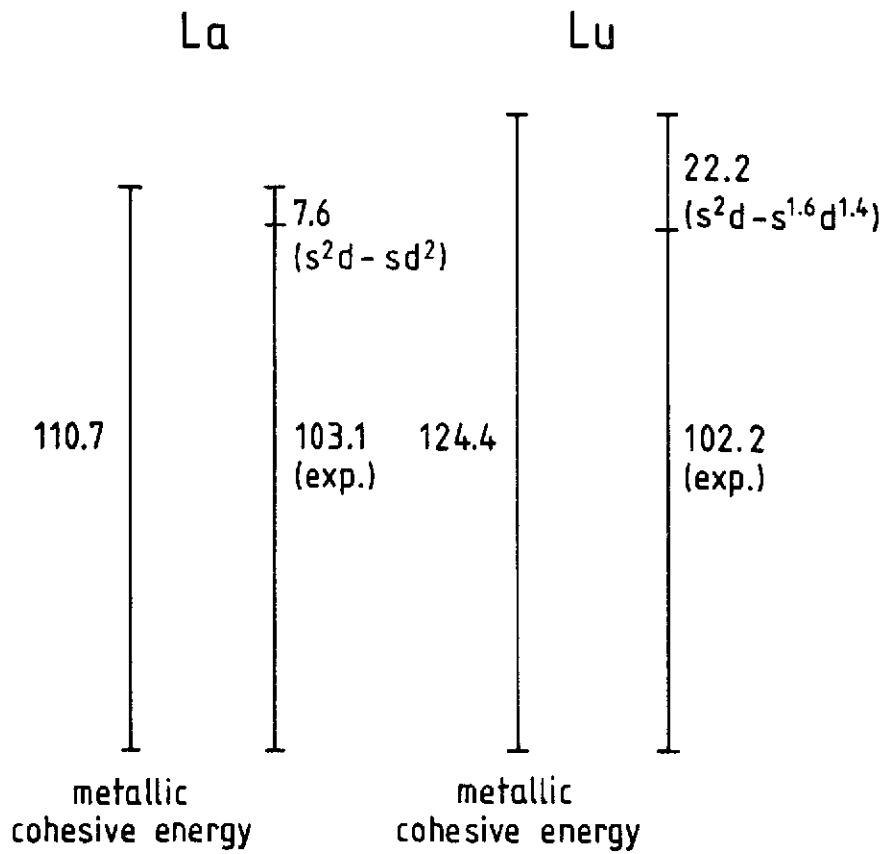


Fig. 2

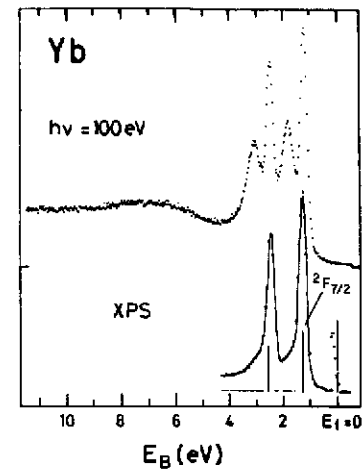
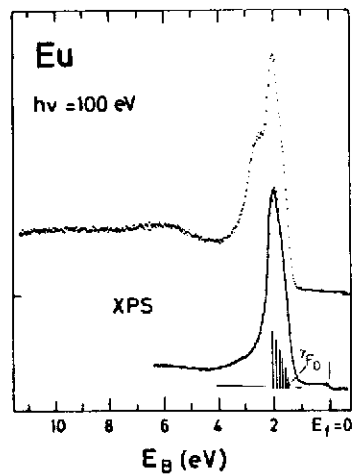
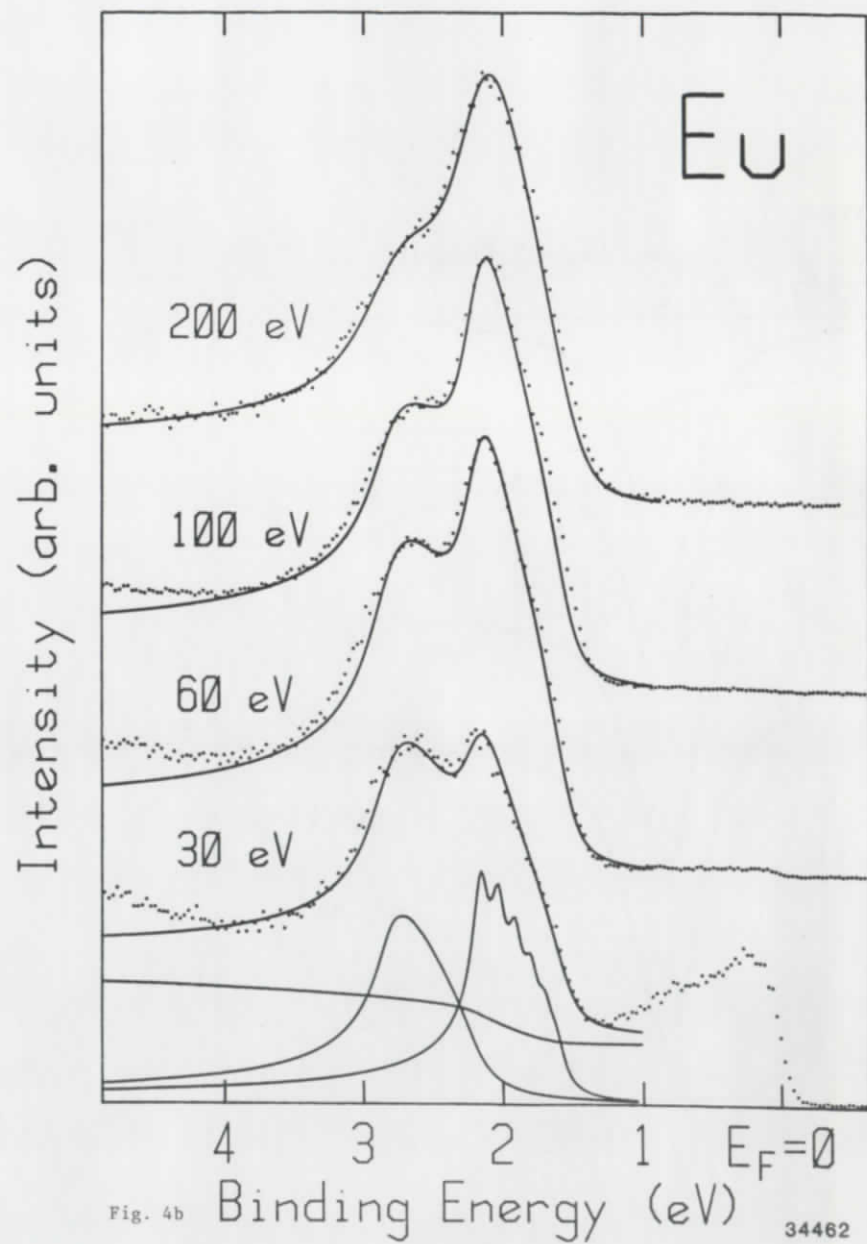
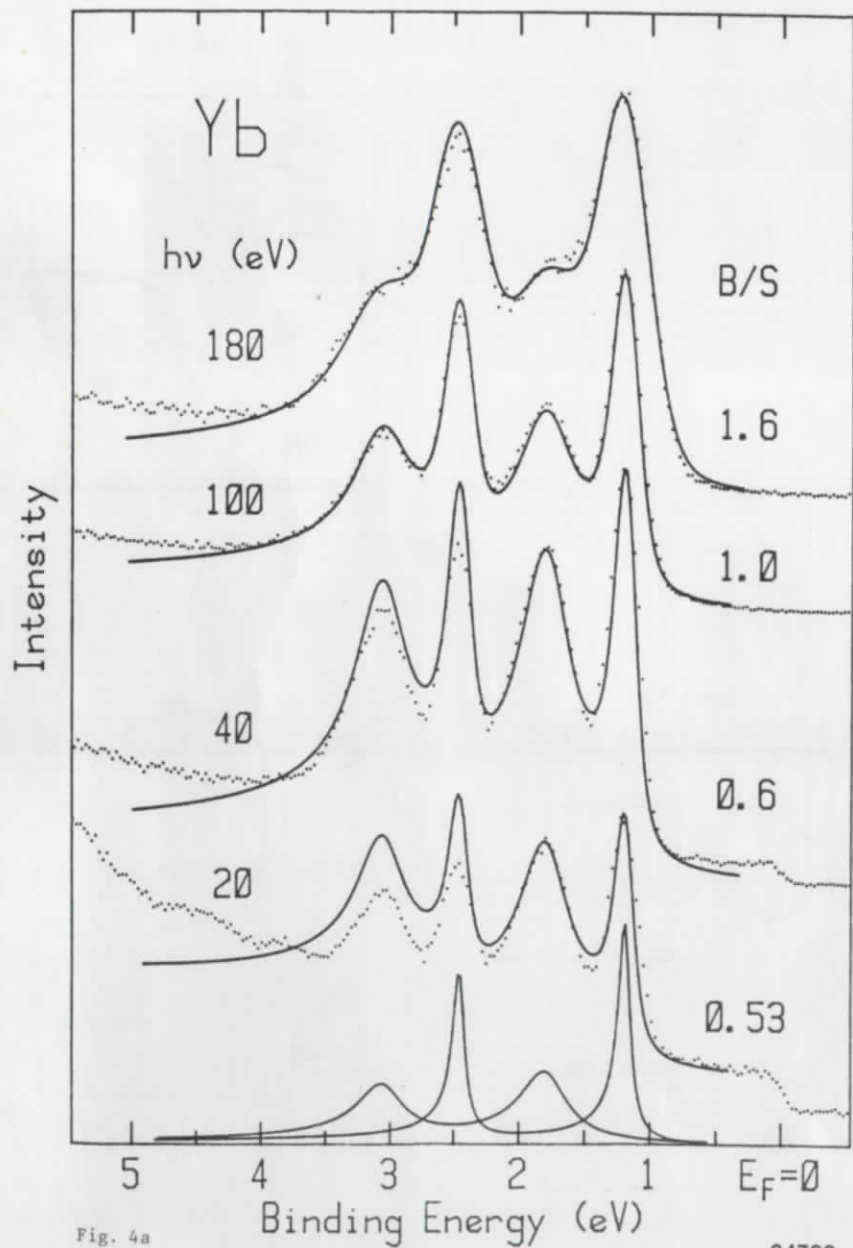


Fig. 3



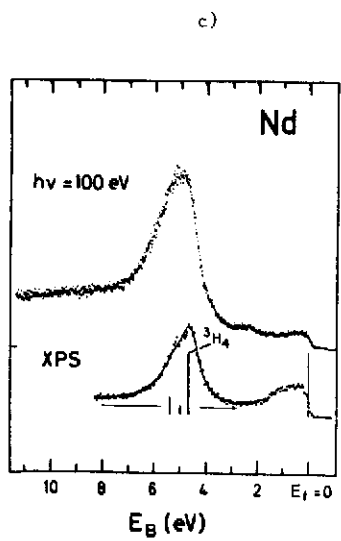
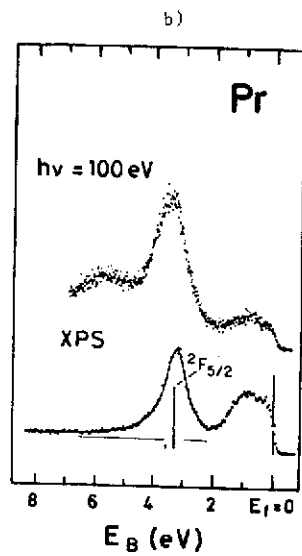
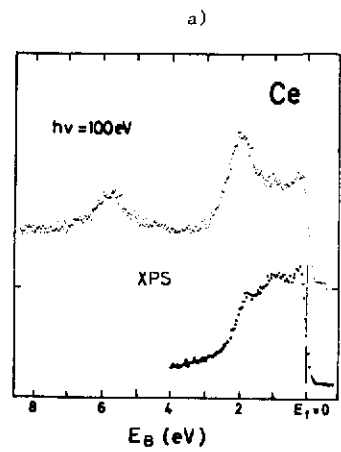


Fig. 5

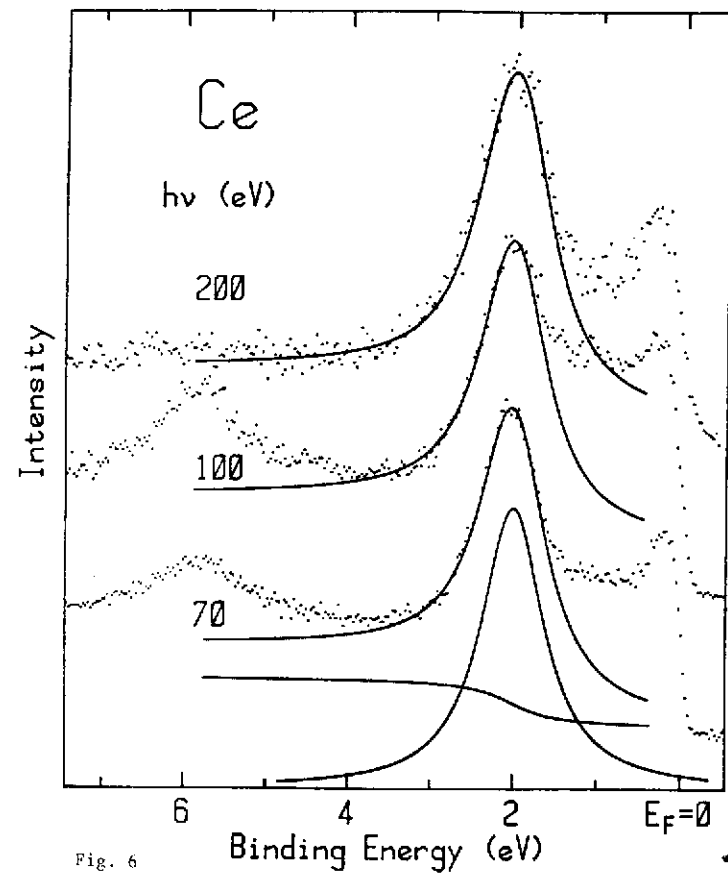
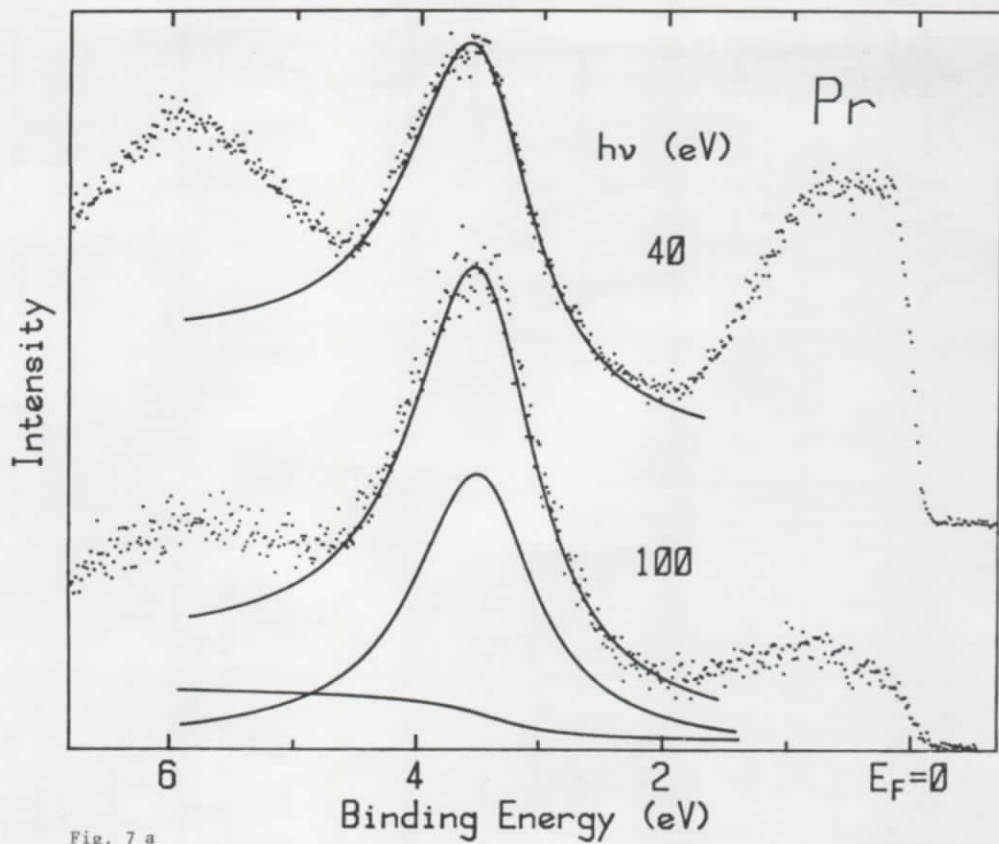
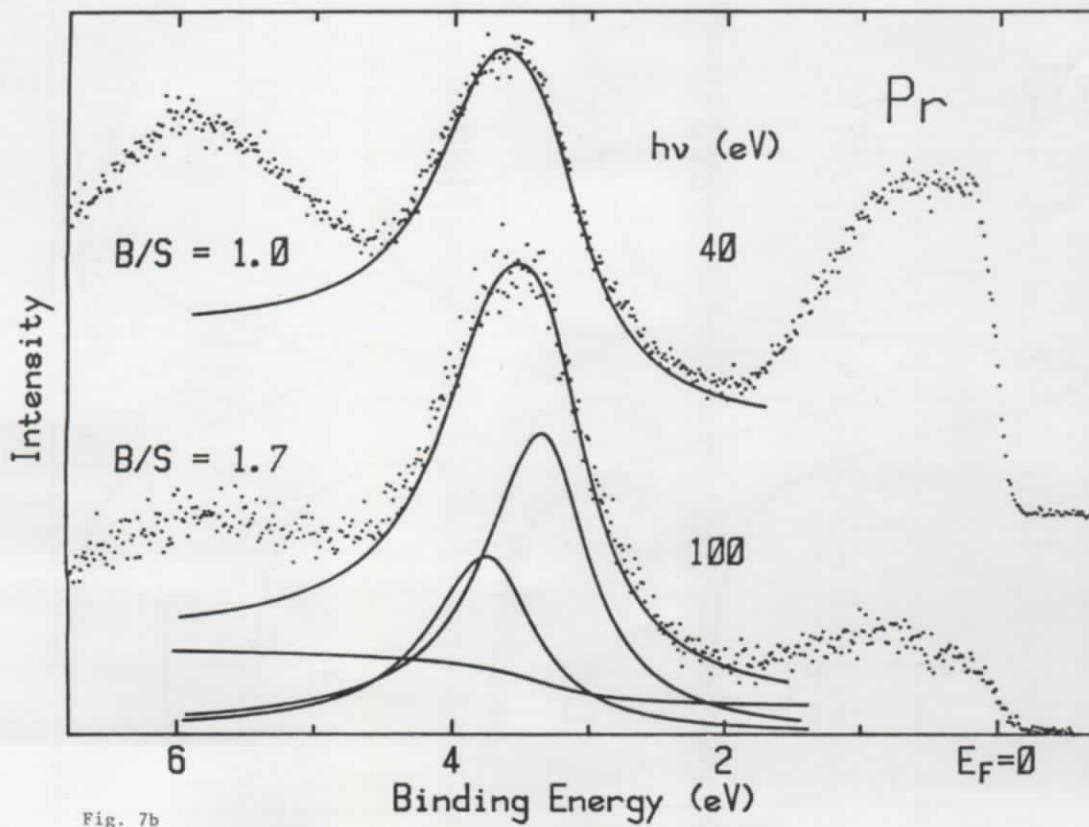


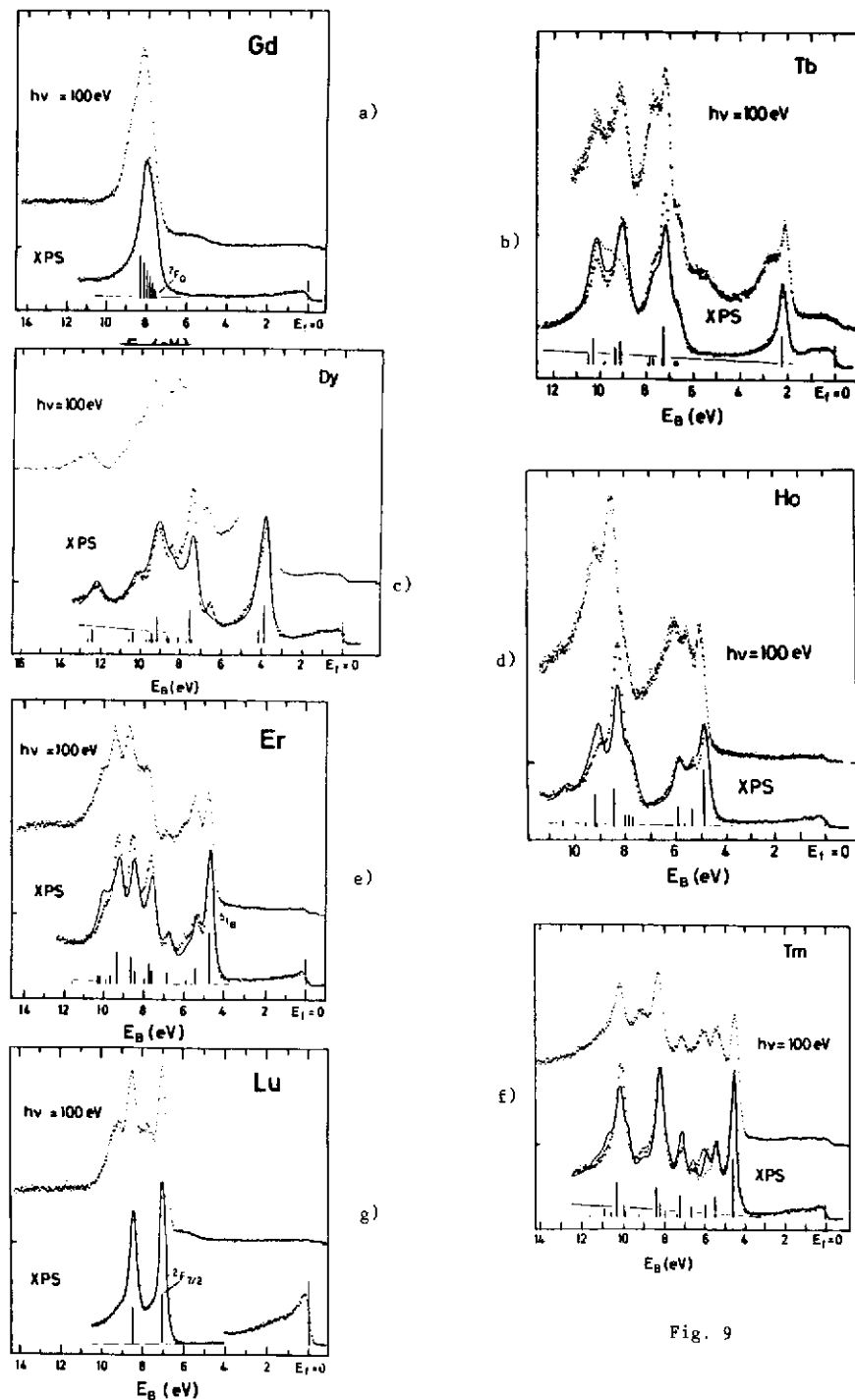
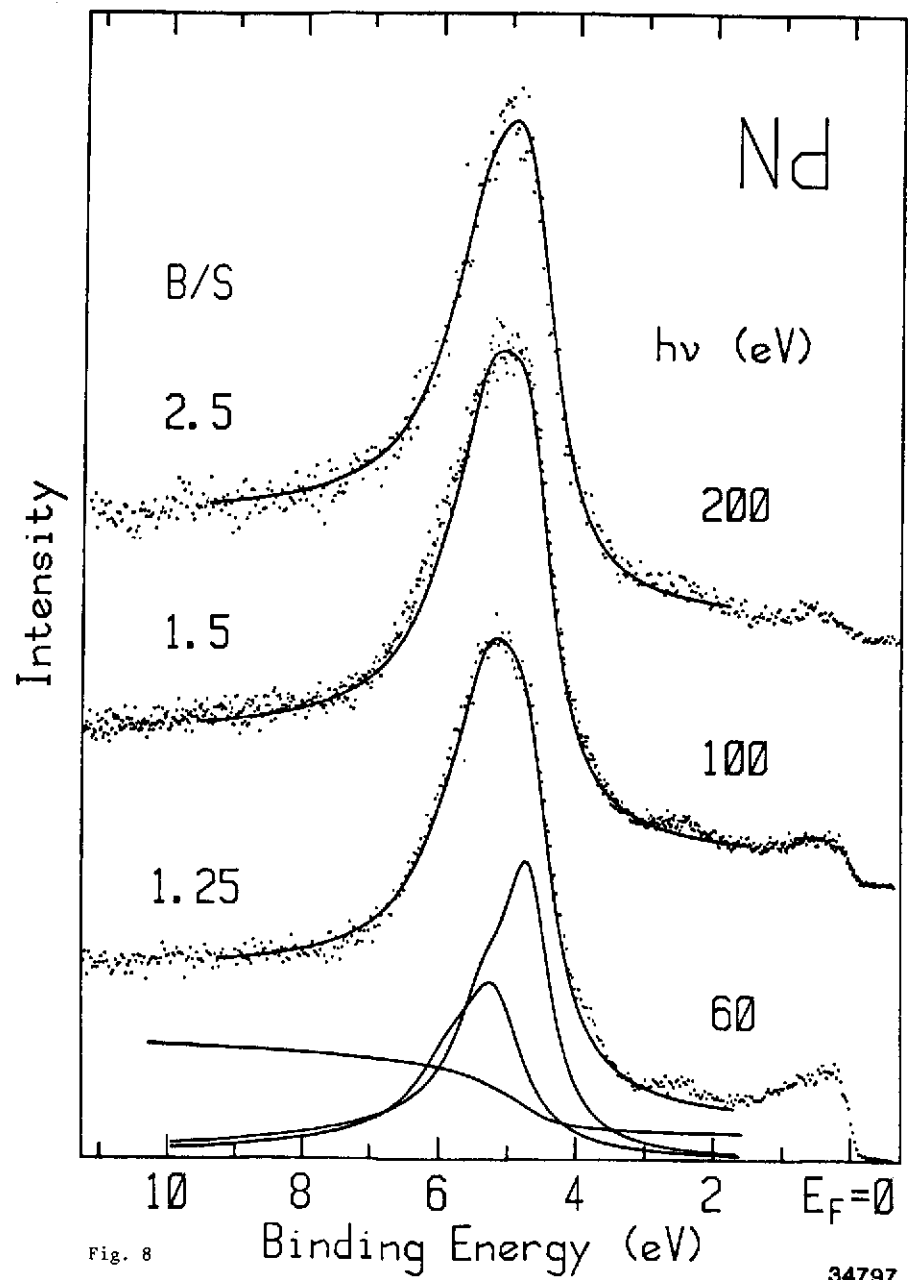
Fig. 6



34745



34746



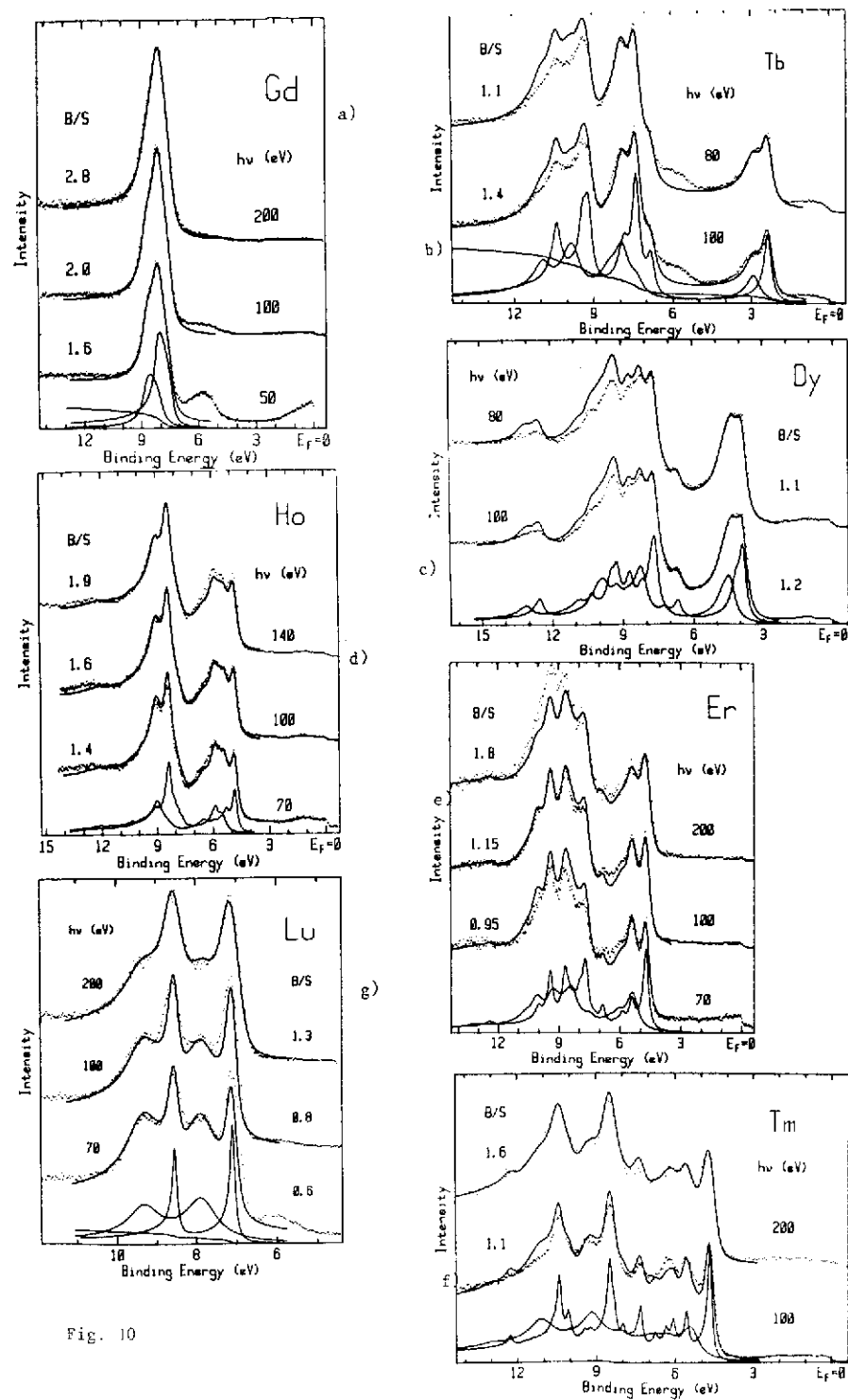


Fig. 10

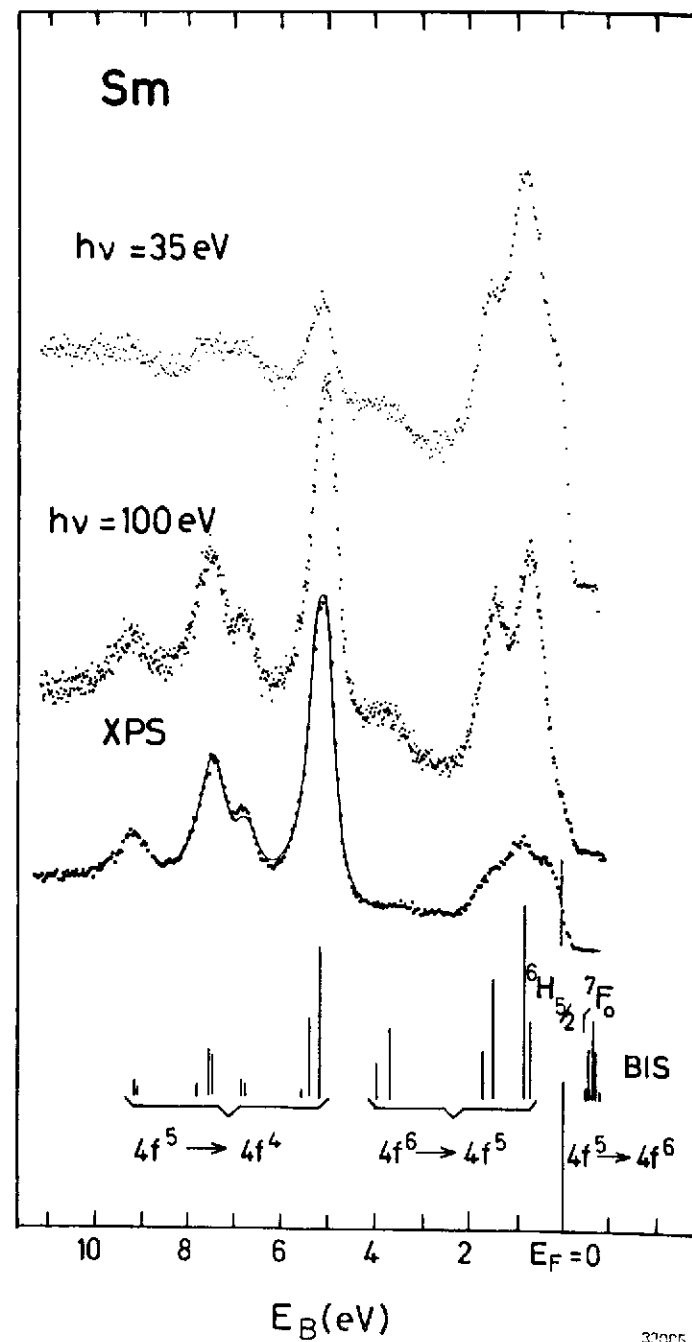


Fig. 11

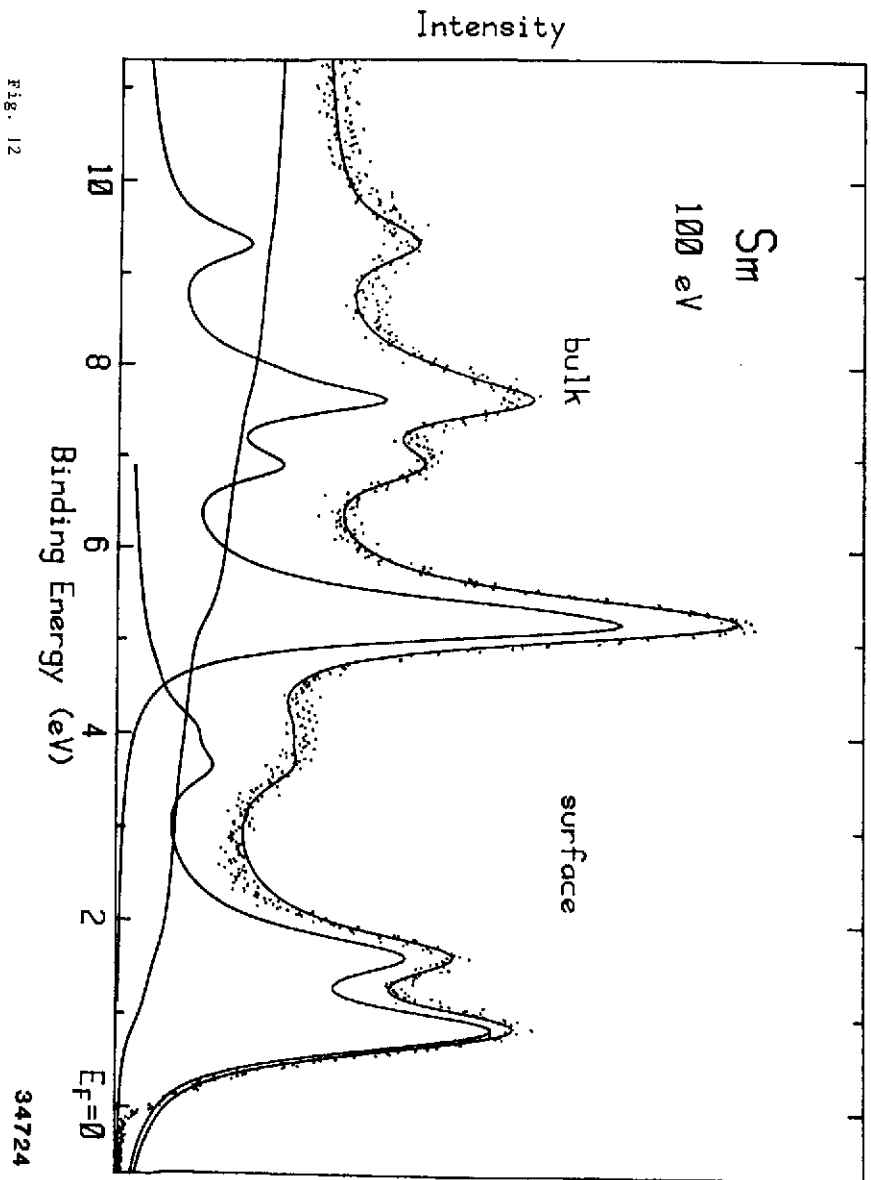
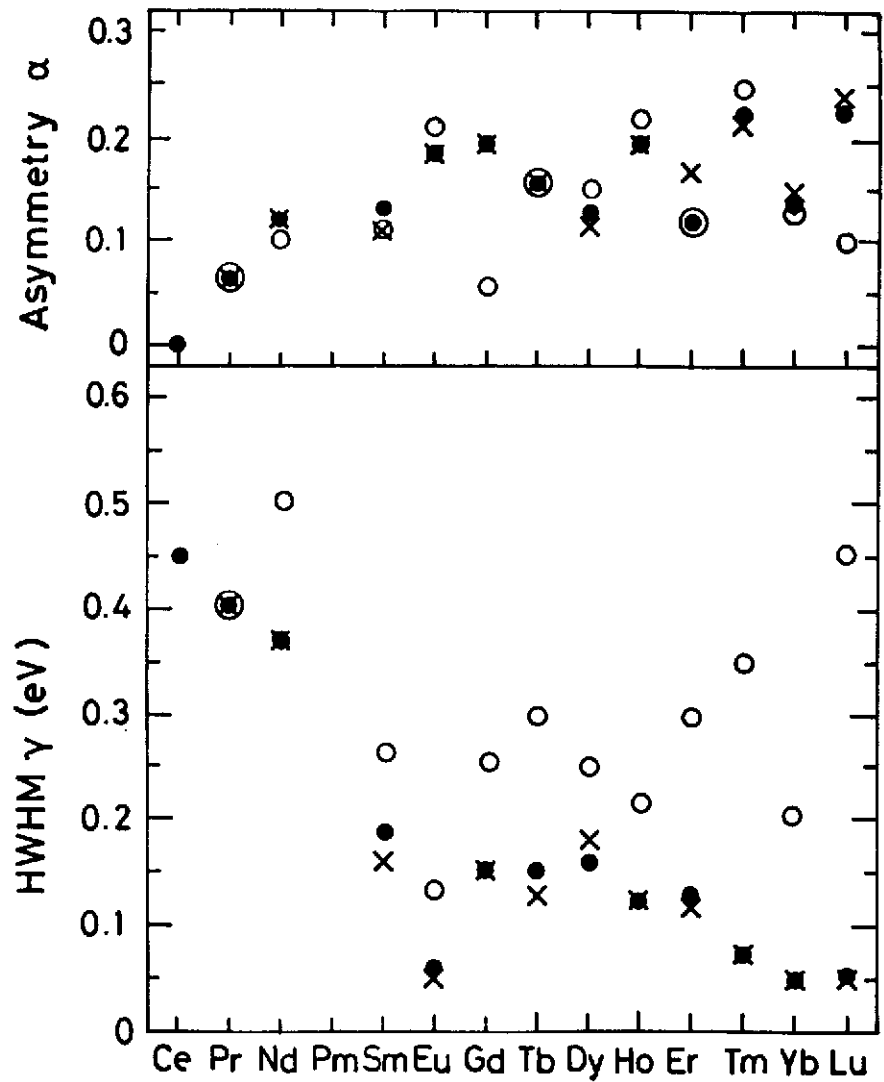


Fig. 12

34724



34721

Fig. 13

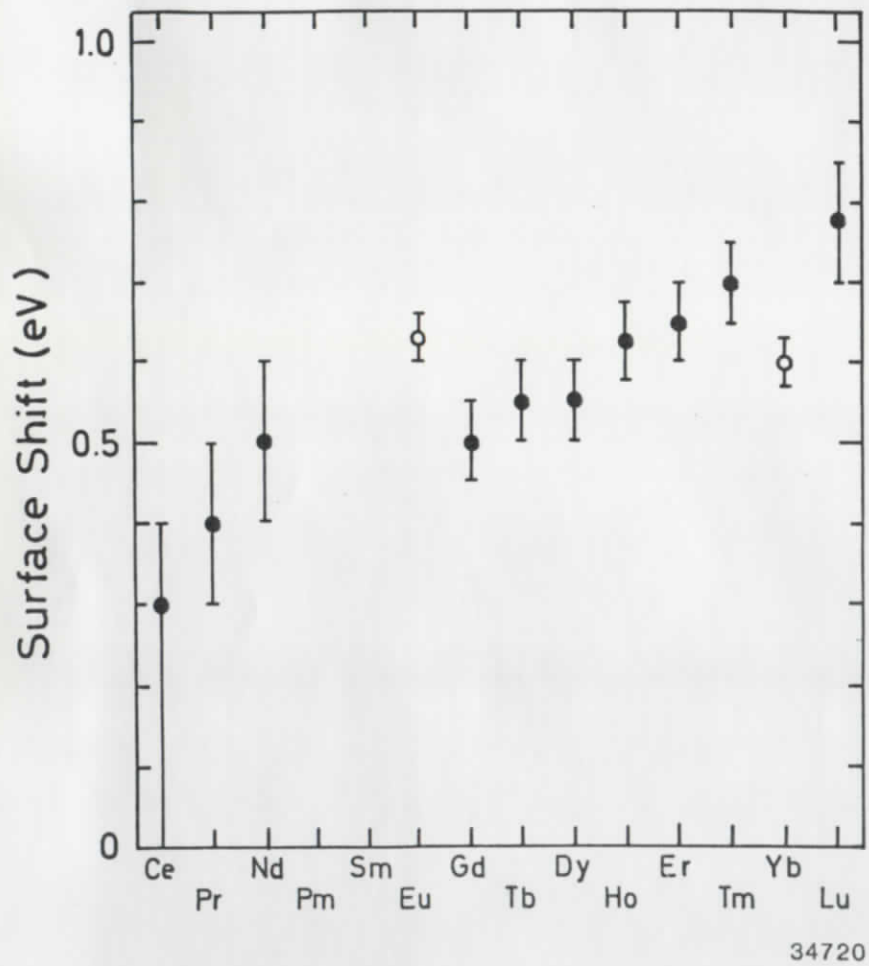


Fig. 14

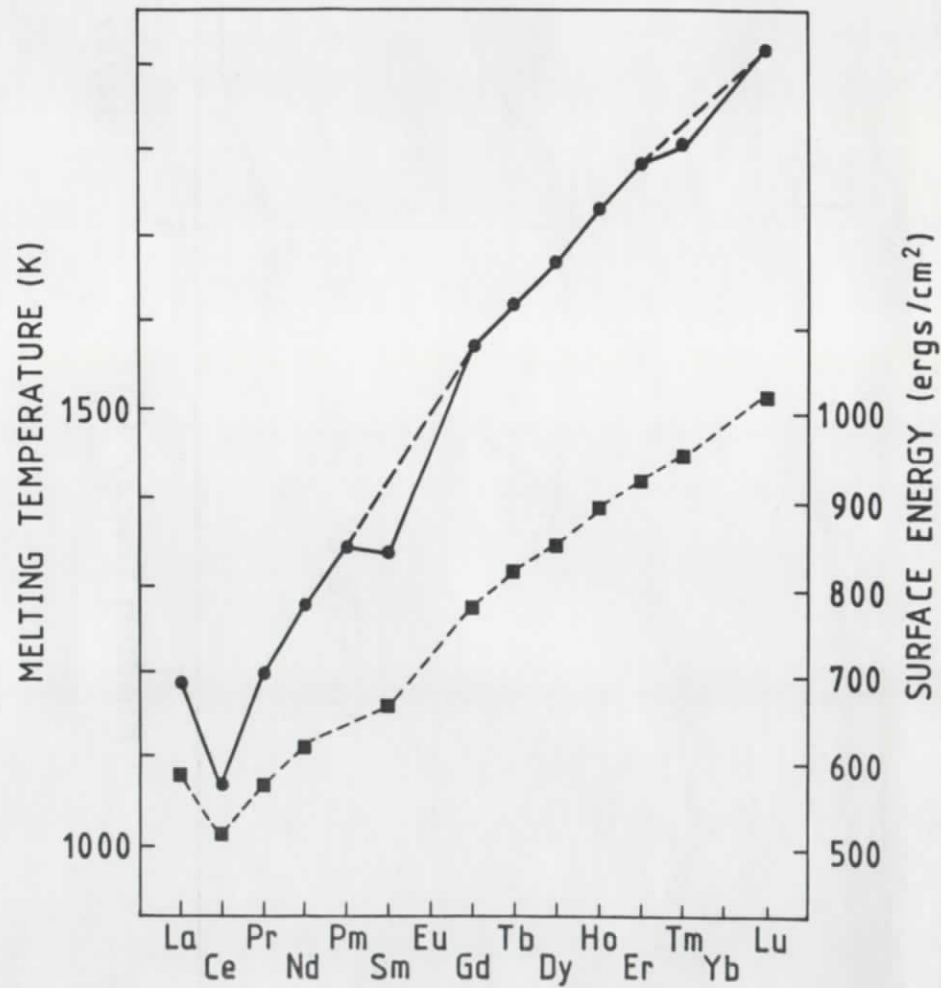


Fig. 15

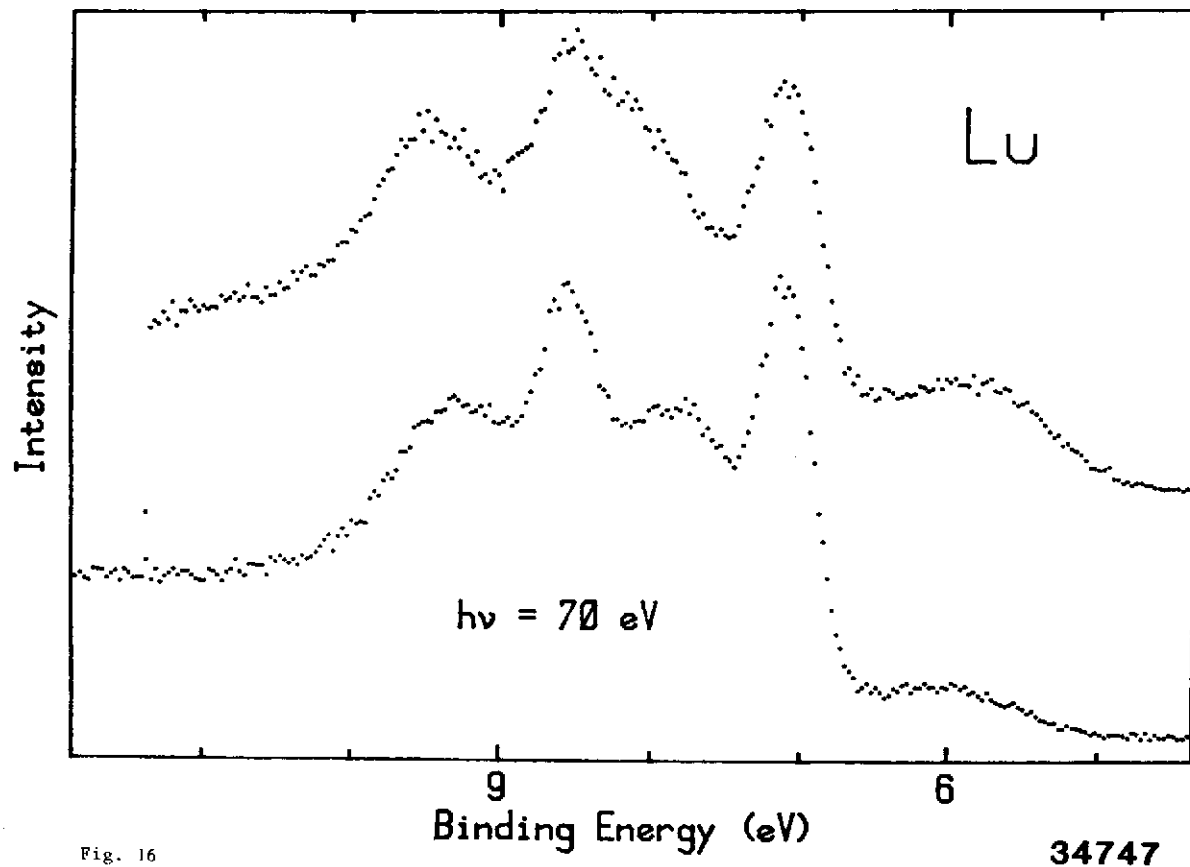


Fig. 16

34747